Title: Therapeutic Modulation of the Immune Response in Arrhythmogenic Cardiomyopathy

Manuscript number: CIRCULATIONAHA/2019/040676R1

Author(s): Jeffrey Saffitz, Beth Israel Deaconess Medical Center
Stephen Chelko, Johns Hopkins University
Angeliki Asimaki, St George's University of London
Justin Lowenthal, Johns Hopkins University School of Medicine, Baltimore, MD
Carlos Bueno-Beti, St George's, University of London, London, UK
Djahida Bedja, Johns Hopkins University School of Medicine
Arianna Scalco, University of Padova
Nuria Amat-Alarcon, Johns Hopkins University School of Medicine
Peter Andersen, Johns Hopkins University School of Medicine

Daniel Judge, Medical University of South Carolina

Leslie Tung, Johns Hopkins University

Therapeutic Modulation of the Immune Response in Arrhythmogenic Cardiomyopathy

Stephen P. Chelko, PhD,[1] Angeliki Asimaki, PhD,[2] Justin Lowenthal, BS,[3]
Carlos Bueno-Beti, PhD,[2] Djahida Bedja, PhD,[1] Arianna Scalco, MS,[4] Nuria Amat-Codina, MS,[1]
Peter Andersen, PhD,[1] Daniel P. Judge, MD,[5] Leslie Tung, PhD,[3] Jeffrey E. Saffitz, MD, PhD [6]

[1] Department of Medicine, Johns Hopkins School of Medicine, Baltimore, MD
[2] St. George's University of London, London, UK
[3] Department of Biomedical Engineering, Johns Hopkins University School of Medicine, Baltimore, MD
[4] Department of Cardiac, Thoracic, Vascular Sciences and Public Health, University of Padova, Padova, Italy
[5] Department of Medicine, Medical University of South Carolina, Charleston, SC
[6] Department of Pathology, Beth Israel Deaconess Medical Center, Boston, MA

Running title: Modulation of Immune Signaling in ACM

Correspondence:

Jeffrey E. Saffitz, MD, PhD
Department of Pathology
Beth Israel Deaconess Medical Center
330 Brookline Ave
Boston, MA 02215
phone: 617-667-4343
fax: 617-667-2943
email: jsaffitz@bidmc.harvard.edu

Abstract

Introduction: Inflammation is a prominent feature of arrhythmogenic cardiomyopathy (ACM), but whether it contributes to the disease phenotype is not known. To define the role of inflammation in the pathogenesis of ACM, we characterized effects of inhibition of inflammatory signaling in ACM models in vitro and in vivo, and in cardiac myocytes from patient induced pluripotent stem cells (hiPSCs).

Results: Activation of NFκB signaling, indicated by increased expression and nuclear accumulation of phospho-RelA/p65, occurs in both an in vitro model of ACM (expression of $JUP^{2157del2}$ in neonatal rat ventricular myocytes), and in a robust murine model of ACM (homozygous knock-in of mutant desmoglein-2; $Dsg2^{mut/mut}$) that recapitulates the cardiac manifestations seen in ACM patients. Bay 11-7082, a small molecule inhibitor of NFκB signaling, prevented development of ACM disease features in vitro (abnormal redistribution of intercalated disk proteins, myocyte apoptosis, release of inflammatory cytokines) and in vivo (myocardial necrosis and fibrosis, LV contractile dysfunction, ECG abnormalities). Hearts of $Dsg2^{mut/mut}$ mice expressed markedly increased levels of inflammatory cytokines and chemotactic molecules which were attenuated by Bay 11-7082. Salutary effects of Bay 11-7082 correlated with the extent to which production of selected cytokines had been blocked. NFκB signaling was also activated in cardiac myocytes derived from a patient with ACM. These cells produced and secreted abundant inflammatory cytokines under basal conditions, and this was also greatly reduced by Bay 11-7082.

Conclusions: Inflammatory signaling is activated in ACM and it drives key features of the disease. Targeting inflammatory pathways may be an effective new mechanism-based therapy for ACM.

Key words: arrhythmogenic cardiomyopathy; inflammation; NFκB signaling; cytokines

Clinical Perspective

What is new?

- NFκB signaling is activated in cardiac myocytes in arrhythmogenic cardiomyopathy.
- Bay 11-7082, a small molecule inhibitor of NFκB signaling, prevents development of major features of the disease phenotype.
- Cardiac myocytes express large amounts of inflammatory cytokines and chemotactic molecules in arrhythmogenic cardiomyopathy reflecting activation of an innate immune response in the heart.

What are the clinical implications?

- Clinically important features of arrhythmogenic cardiomyopathy - myocardial injury and arrhythmias - are driven by activation of an immune response in the heart.
- Anti-inflammatory drug therapy may be an effective, mechanism-based strategy to reduce myocardial damage and risk of sudden death in patients with arrhythmogenic cardiomyopathy.

Introduction

Arrhythmogenic cardiomyopathy (ACM) is a familial non-ischemic heart muscle disease that causes sudden death in the young and especially in athletes.[1-3] The only strategy proven to prevent sudden death in ACM patients at risk is an implantable cardiac defibrillator. No mechanism-based drug therapies are currently available.

Molecular mechanisms responsible for the pathogenesis of ACM are incompletely understood. However, considerable evidence implicates abnormal signaling by glycogen synthase kinase-3β (GSK3β) in ACM.[4-6] A small molecule, SB216763, annotated as an inhibitor of GSK3β,[7] prevents and/or reverses the ACM disease phenotype (including redistribution of cell-cell junction proteins in cardiac myocytes, arrhythmias, exercise-induced sudden death, ventricular myocyte injury and apoptosis, and contractile dysfunction) in ACM models in vitro, in zebrafish and mouse models in vivo, and in buccal mucosa cells and hiPSC-cardiac myocytes derived from ACM patients.[6,8,9] The key insight to emerge from studies in vivo is that the clinically important features of the disease phenotype – arrhythmias and myocardial damage – arise via a common disease mechanism that can be blocked by a single small molecule. However, effective mechanism-based drug therapy of ACM to reduce sudden death will likely require chronic administration, and long-term inhibition of GSK3β and its effects on Wnt/β-catenin signaling pathways could have unacceptable adverse consequences including increased risk of developing cancer.[10] Thus, to identify potential new targets for drug therapy, we looked downstream of GSK3β and focused on inflammatory signaling.

Inflammation has long been recognized as a feature of ACM.[11,12] First described by autopsy pathologists,[12] inflammatory infiltrates occur in the hearts of 60 to 88% of ACM patients, and are especially common in ACM patients who died suddenly.[12,13] They are often seen in both ventricles even when macroscopic disease is confined to the right ventricle.[13] It has been suggested that a histologic picture reminiscent of acute myocarditis may reflect an active phase of ACM associated with accelerated disease progression.[14] It has also been shown that ACM patients have elevated circulating levels of pro-

inflammatory cytokines, and cardiac myocytes themselves produce potent cytokines in ACM.[15] Thus, inflammation in ACM involves infiltrating inflammatory cells *and* activation of an innate immune response in cardiac myocytes, one or both of which could contribute to disease onset and progression. However, the role of inflammation as a driver of the ACM disease phenotype has not been studied previously.

NFκB is a master regulator of cellular inflammatory responses initiated by diverse injurious agents including stress, pro-inflammatory cytokines, reactive oxygen species, heavy metals, UV radiation, oxidized LDL and bacterial/viral antigens.[16,17] There are clear links between GSK3β and NFκB signaling pathways, and abundant evidence indicates that activation of GSK3β promotes inflammation through NFκB, whereas inhibition of GSK3β limits inflammation.[18-21] Accordingly, we tested the hypothesis that inflammatory signaling mediated by NFκB promotes myocardial damage, contractile dysfunction and cytokine production in ACM. Here, we show that NFκB signaling is activated in ACM. Moreover, inhibition of inflammatory signaling with a small molecule inhibitor of NFκB shows a remarkable ability to rescue the disease phenotype in ACM models in vitro and in vivo involving expression of three different alleles known to cause disease in patients.

Materials and Methods

Transparency and Openness Promotion

The data that support the findings of this study are available from the corresponding author upon reasonable request.

Animal Studies

All animal studies were in full compliance with policies of Beth Israel Deaconess Medical Center, Johns Hopkins School of Medicine and St. George's University of London. They also conformed to the *Guide for the Care and Use of Laboratory Animals* from the National Institutes of Health (NIH publication no. 85-23, revised 1996). In vitro studies involved transfection of cultured

neonatal rat ventricular myocytes with a mutant allele of the desmosomal protein plakoglobin (*JUP*^{2157del2}) as previously described.[7] In vivo studies were performed in mice with homozygous knock-in of a mutant form of *Dsg2*, the gene encoding the desmosomal cadherin desmoglein-2 (*Dsg2*$^{mut/mut}$ mice) as previously described.[6] This mutation entails loss of exons 4 and 5 which causes a frameshift and premature termination of translation.

Preparation of primary cultures of neonatal rat ventricular myocytes

Primary cultures were prepared from disaggregated ventricles of 1-day-old Wistar rat pups (Charles River) as previously described.[7] At 24 hours post-seeding, cultures were transfected with an adenoviral construct expressing plakoglobin with the 2157del2 mutation (*JUP*^{2157del2}), as previously reported .[7] At 24 hours post-transfection, cultures were treated with Bay11-7082 (Sigma, 5μM) for an additional 24 hours. This concentration of Bay 11-7082 has been used in numerous in vitro studies to inhibit NFκB signaling (see [22,23] for example). Transfected cultures treated with vehicle only (DMSO) and non-transfected cultures were used for control purposes.

In vivo drug treatment

Four cohorts of mice at 8 weeks of age were anesthetized and implanted with subcutaneous osmotic mini-pumps (Alzet, Model 1004). These included: 1) *Dsg2*$^{mut/mut}$ mice with pumps containing 50μg/μL Bay11-7082 in a vehicle of 65% DMSO, 15% ethanol, and 20% saline; 2) *Dsg2*$^{mut/mut}$ mice with pumps containing an equivalent volume of vehicle; 3) wildtype mice with pumps containing 50μg/μL Bay11-7082 in a vehicle of 65% DMSO, 15% ethanol, and 20% saline; and 4) wildtype mice with pumps containing an equivalent volume of vehicle. Mice in cohorts 1 and 3 received 5mg/kg/day of Bay11-7082 by continuous infusion; those in cohorts 2 and 4 received an equivalent volume of vehicle each day for 4 weeks. At 12 weeks of age, mice were re-anesthetized and new Alzet pumps were implanted for an additional 4 weeks of treatment. This dose of Bay 11-7082 has been shown in numerous studies to block NFκB signaling in vivo.[24-27]

Mouse echocardiography and electrocardiography

At the end of the 8 week drug treatment protocol, cardiac function was assessed in all mice by transthoracic echocardiography and electrocardiography (ECG) as previously described.[6] Echocardiographic measurements were made according to American Society of Echocardiography guidelines [28] in non-sedated mice using a Vevo 2100 Visualsonic imaging system. Parasternal long-axis views of the left ventricle (LV), at the level of the papillary muscles, were acquired at a sweep speed of 200 mm/second. Three to five measurements were acquired from each mouse and averaged to assess LV function as previously described.[6] ECG measurements made in anesthetized mice in which wire electrodes had been sutured in place in the right and left arms to obtain standard lead I ECG recordings. Recordings were captured via PowerLab and analyzed via the LabChart Pro *ECG Analysis Add-on Software* (LabChart Pro 8, MLS360/8, AD Instruments). ECGs were recorded for 15 minutes and all ECG wave and amplitude parameters were analyzed as signal averaged ECGs (SAECGs). Following completion of functional studies, mice were euthanized and hearts were excised and processed for additional studies either by freezing fresh tissue (-80C) or fixing tissue in 10% buffered formalin and embedding in paraffin.

hiPSC-cardiac myocyte differentiation and Bay11-7082 treatment

These studies involved a previously characterized hiPSC line from an ACM patient with a c.2013delC (p.Lys672Argfs*12) mutation in plakophilin-2 (*PKP2*) originally produced by Joseph Wu at Stanford and described previously,[8] and an unrelated healthy control hiPSC line previously derived at Johns Hopkins by Gordon Tomaselli and colleagues.[29] Stem cell lines were cultured as monolayers and differentiated into cardiac myocytes according to a published protocol with minor modifications.[30] Briefly, hiPSCs were plated in 6-well culture plates coated with 1:200 Geltrex LDEV-free reduced growth factor matrix:DMEM/F-12 with HEPES (both Gibco). They were maintained for the first 18 hours in Essential 8 medium (E8, Gibco) with 10 μM Y-27632 dihydrochloride (Tocris Bioscience,

Bristol, UK), and then subsequently fed daily with E8 medium for a total of four days. Cells were plated at a density sufficient to produce 70-90% confluence at 4 days, at which time differentiation was initiated (defined as day 0 or "d0").

On d0, E8 media was replaced with RPMI 1640 medium supplemented with B-27 supplement minus insulin (Gibco) and 6 μM CHIR-99021 (Selleck Chemicals, Houston, TX) to initiate differentiation. Thereafter, media was changed as follows: RPMI 1640 medium with B-27 supplement (minus insulin) on d2, RPMI 1640 medium with B-27 supplement (minus insulin) and 5 μM IWR-1 (Sigma-Aldrich Corp., St. Louis, MO) on d3, RPMI 1640 medium with B-27 supplement (minus insulin) on d5 and d7, and RPMI 1640 medium with B-27 supplement (with insulin) on d9 and beyond. Spontaneous beating was first observed at d7-9. At d13-15, cells were dissociated using 0.05% trypsin-EDTA, mixed and re-plated on fresh Geltrex-coated 6 well plates. They were then metabolically-purified using lactate supplemented glucose-free DMEM/F12 for 4 days, with media changed every other day. Cells were then switched back to B-27 supplemented-RPMI and either maintained for further use or cryopreserved.

On day 30 from the start of differentiation, myocytes were plated at a density of 300,000 cells/cm^2 to produce confluent monolayers in 12-well plates or on Thermanox coverslips in 24-well plates, both coated with 1:200 Geltrex:DMEM/F12. They were cultured in B-27 supplemented-RPMI for 1 week and allowed to form a contracting syncytium. Half of the wells were treated with Bay 11-7082 (10μM) for 8 days, with media replaced every other day. Media removed at each change was stored at -80C for subsequent cytokine assays. At day 8, cells were lysed with TRIzol Reagent (Ambion, Life Technologies) and the lysate was stored at -80°C for cytokine assays.

Cytokine assays in mouse hearts and patient hiPSC-Cardiac myocytes

Myocardium from mice was lysed in RIPA buffer and cardiac myocytes from patient hiPSCs were lysed in TRIzol, and protein in lysates was quantified by standard BCA protein assay. Mouse (R&D

Systems, Cat. No. ARY028) and Human (R&D Systems, Cat. No. ARY022B) Proteome Profiler XL Cytokine Arrays were blocked at room temperature for 1hour before being incubated overnight at 4°C with 200 µg of myocardial protein in blocking buffer supplied by manufacturer. Additional arrays were incubated overnight at 4°C with 200 µl of hiPSC-cardiac myocyte culture medium according to the manufacturer's protocol for cell supernatants. Following overnight incubation, arrays were washed four times (10 minutes/wash), incubated at room temperature for 1 hour with Antibody Detection Cocktail, washed an additional four times (10 minutes/wash), then incubated with 1:2,000 Streptavidin-HRP in blocking buffer for 30 minutes at room temperature. Arrays were then washed four times, and chemiluminescence was performed using the Chemi Reagent Mix included in the assay kits.

Statistical Analysis

Data are presented as mean ± SEM. Specific n-values and descriptions of statistical analyses are included in legends for each figure and table. $P<0.05$ was considered statistically significant. Differences in measured variables were assessed using one-way analysis of variance (ANOVA) with Tukey's post-hoc analysis to correct for multiple comparisons. In view of sample sizes, Gaussian distributions were assumed. Pearson's correlation coefficients (r) were calculated to determine correlations between (i) percent ejection fraction and percent myocardial fibrosis and apoptosis; and (ii) expression levels of selected cytokines and percent ejection fraction. Pearson's correlation matrix tables were constructed to correlate the expression level of each individual cytokine with expression levels of all other cytokines. All statistical analyses were validated by a biostatistician from the Johns Hopkins Institute for Clinical and Translational Research (ICTR) Biostatistics Core and analyzed with Prism 7 GraphPad Software.

Other Methods

Descriptions of methods for in vitro immunofluorescence, in vitro apoptosis assays, in vitro cytokine assays, quantification of myocardial fibrosis, mouse myocardial tissue immunofluorescence

and immunoperoxidase, and total RelA/p65 and phospho-RelA/p65 western blots are included in on-line supplemental files for this paper.

Results

Inhibition of NFκB signaling reverses ACM disease features in vitro

Primary cultures of neonatal rat ventricular myocytes that express a mutant form of the desmosomal protein plakoglobin (*JUP*^{2157del2}), known to cause ACM in patients,[31] exhibit several features in vitro that are also seen in the hearts of ACM patients.[6,8,9,15,32] These include redistribution of plakoglobin (also known as γ-catenin) from cell-cell junctions into the cytosol and nucleus; loss of cell-surface immunoreactive signal for the major cardiac gap junction protein, connexin43 (Cx43); redistribution of GSK3β from the cytosol to the cell surface; and myocyte apoptosis. We have shown previously that all of these features are normalized when transfected cells are incubated with SB216763, which inhibits GSK3β.[6,8] We now show in **Figure 1A** that immunoreactive signal for phospho-RelA/p65 (Ser536) accumulates in the nuclei of cardiac myocytes expressing *JUP*^{2157del2}, indicating activation of NFκB signaling in this in vitro model of ACM. Treatment of these cells with Bay 11-7082 prevented nuclear accumulation of phospho-RelA/p65, thus confirming that this small molecule inhibits NFκB signaling (**Figure 1A**). Furthermore, incubation of these ACM cardiac myocytes with Bay 11-7082 for 24 hours normalized the aberrant distribution of key proteins (**Figure 1B**). The pattern of distribution of plakoglobin, Cx43 and GSK3β in treated cells was indistinguishable from that seen in control (non-transfected) cardiac myocytes (**Figure 1B**). In addition, myocyte apoptosis, measured by TUNEL labeling, was increased by roughly 10-fold in ACM myocytes but returned to control levels after exposure to Bay 11-7082 for 24 hours (**Figure 1C and D**). Treatment of control (non-transfected) neonatal rat ventricular myocytes with Bay 11-7082 under identical conditions had no apparent effect on the distribution of immunoreactive signals for phospho-RelA/p65 (Ser536), N-cadherin, plakoglobin, Cx43 or GSK3β, and no effect on myocyte apoptosis (**Supplemental Figure 1**).

We have reported previously that expression of *JUP*^{2157del2} causes neonatal rat ventricular myocytes to produce and secrete cytokines into the culture media.[8] A repeat of these studies confirmed that cells expressing mutant plakoglobin produce and secrete a wide variety of inflammatory cytokines and chemoattractant molecules (**Figure 2**). In addition, we now show that incubating these cells with Bay 11-7082 for 24 hours greatly reduces accumulation of these factors in the culture media and produces a picture nearly identical to that seen in control (non-transfected) myocytes (**Figure 2**). Because these cultures contain no leukocytes and consist of >90% cardiac myocytes, these observations indicate that *JUP*^{2157del2} stimulates secretion of inflammatory mediators by cardiac myocytes under the control of NFκB.

Inhibition of NFκB signaling prevents development of ACM disease features in vivo

To determine if NFκB signaling is activated in the hearts of *Dsg2*$^{mut/mut}$ mice, we performed western blots to measure expression levels of total RelA/p65 and phospho-RelA/p65 (Ser536) in myocardial homogenates. As shown in **Figure 3A and B**, the amount of total myocardial RelA/p65 was equivalent in control (wildtype) and *Dsg2*$^{mut/mut}$ mice, but the amount of phospho-RelA/p65 was significantly increased in the hearts of *Dsg2*$^{mut/mut}$ mice. Treatment of *Dsg2*$^{mut/mut}$ mice with Bay 11-7082 reduced the amount of phospho-RelA/p65 to levels equivalent to that seen in control hearts. These observations indicate that NFκB signaling is activated in the hearts of *Dsg2*$^{mut/mut}$ mice and Bay 11-7082 acts to block this signaling pathway.

Next, to determine if inhibition of inflammatory signaling mitigates development of the ACM phenotype in vivo, we treated *Dsg2*$^{mut/mut}$ mice with Bay 11-7082 by continuous infusion over an 8 week period beginning when the mice were 8 weeks of age. As reported previously,[6] *Dsg2*$^{mut/mut}$ mice show little if any apparent cardiac structural or functional derangements at 8 weeks of age, but during the ensuing 8 weeks, they develop a robust phenotype that recapitulates the most important clinical features seen in ACM patients, namely myocardial damage and arrhythmias. This includes progressive

deterioration of ventricular contractile function associated with development of extensive myocardial necrosis, fibrosis and inflammation. It also includes ECG abnormalities and arrhythmias. These structural and functional changes are associated with marked shifts in the distribution of various cardiac myocyte proteins including desmosomal proteins, connexins and ion channel proteins, proteins involved in the Wnt/β-catenin signaling pathway, and synapse associated protein 97 (SAP97), a chaperone protein involved in ion channel transport to intercalated disks.[6,8] As shown in **Figure 3C-J**, treatment of *Dsg2*$^{mut/mut}$ mice with Bay 11-7082 substantially mitigated this phenotype. Contractile function was normalized and there was a marked reduction in the amount of ventricular myocardial necrosis and fibrosis, along with a significant reduction in the number of apoptotic cells seen by TUNEL labeling. Abnormalities in the signal averaged ECG were also corrected. Finally, abnormal distributions of plakoglobin, Cx43, GSK3β and SAP97, which also occur in patients with ACM,[6,8,32] were fully corrected in *Dsg2*$^{mut/mut}$ mice treated with Bay 11-7082. Treatment of control (wild type) mice with Bay 11-7082 by continuous infusion for 8 weeks had no effect on cardiac structure or function (**Supplemental Figure 2**). There was no histologic evidence of myocardial fibrosis or inflammation, and LV ejection fraction and other echocardiographic measures of contractile function were normal. Quantitative data for all morphologic, echocardiographic and electrocardiographic parameters measured in all mouse cohorts are shown in **Table 1**.

Cytokines are produced by cardiac myocytes and infiltrating inflammatory cells in ACM

To characterize production of chemical mediators of the immune response in ACM, we used arrays to measure 111 different cytokines in the hearts of *Dsg2*$^{mut/mut}$ mice and compared the amounts to those measured in the hearts of WT mice and *Dsg2*$^{mut/mut}$ mice treated with Bay 11-7082. We observed substantial expression of multiple cytokines in the hearts of *Dsg2*$^{mut/mut}$ mice. **Figure 4** shows data for selected cytokines (the complete data set is included in **Supplemental Table 1**). Powerful inflammatory mediators were expressed in *Dsg2*$^{mut/mut}$ hearts including IL-1β (up by ~13-fold compared to WT hearts),

IFNγ (~5-fold), IL-12 (~6-fold) and TNFα (~2-fold). Similarly, various chemotactic molecules were greatly increased in *Dsg2*$^{mut/mut}$ hearts compared to WT hearts, including the B-cell chemoattractant CXCL13 (up by ~6-fold), M-CSF (~20-fold), and the neutrophil chemoattractant LIX (CXCL5; ~60-fold). And, expression of various pleomorphic molecules with multiple actions was also greatly increased including HGF (~15-fold) and P-selectin (~40-fold). Finally, there were increases in some molecules that fulfill anti-inflammatory roles such as IL-1Ra (up by ~4-fold). In most, but not all, cases increased expression of these molecules in *Dsg2*$^{mut/mut}$ hearts was blunted or fully normalized by treatment with Bay 11-7082 (**Figure 4**).

Expression of chemical mediators of the immune response is generally considered to be the province of the professional cells of the adaptive immune system, mainly lymphocytes and macrophages. However, parenchymal cells of most organs, including cardiac myocytes, are capable of producing inflammatory mediators, and we know from the in vitro studies shown in Figure 2 that neonatal ventricular myocytes that express mutant plakoglobin produce and secrete diverse cytokines. To identify the cellular source of cytokines in *Dsg2*$^{mut/mut}$ mice, we stained sections of myocardium with antibodies against representative key molecules including IL-1β, TNFα and MCP-1α. As shown in **Figure 5**, positive immunoreactive signal for IL-1β, TNFα and MCP-1α was apparent in cardiac myocytes and signal for IL-1β and TNFα was seen in infiltrating mononuclear inflammatory cells in *Dsg2*$^{mut/mut}$ hearts. Signal intensity in both myocytes and inflammatory cells was reduced in mice treated with Bay 11-7082. From the cytokine assays shown in **Figure 4**, expression of IL-1β and TNFα in the hearts of *Dsg2*$^{mut/mut}$ mice suggests a role for monocyte/macrophages and expression of IFNγ suggests a role for T-cells. In fact, both macrophages and T-cells were present in the inflammatory cells infiltrating the hearts of *Dsg2*$^{mut/mut}$ mice (**Figure 5**). Taken together with data in Figure 2, these observations indicate that inflammation in ACM involves activation of an innate immune response in cardiac myocytes driven, at least in part, by NFκB signaling. Treatment of *Dsg2*$^{mut/mut}$ mice with Bay 11-7082

not only reduced overall cytokine production (as shown in **Figure 4**), but also reduced the total number of infiltrating inflammatory cells in the heart based on a careful survey of myocardial sections.

Prevention of ACM disease features correlates with reduction in cytokine expression

Data shown in Figures 2-5 clearly implicate activation of an immune response in the development of the ACM disease phenotype in *Dsg2*$^{mut/mut}$ mice. However, this does not prove that immune signaling and production of cytokines are directly responsible for driving this phenotype. Nevertheless, we were able to gain further insight into this potential causal relationship by correlating the extent to which Bay 11-7082 mitigated the disease phenotype in individual animals. For example, 3 of 17 treated ACM mice failed to respond to NFκB inhibition. On further investigation, we discovered this was related to a technical failure of drug delivery by implanted Alzet minipumps. As shown in **Figure 6,** these 3 mice (non-responders) had worse cardiac function (i.e., lower ejection fractions) than the other Bay11-7082-treated mice (responders) in this experiment, in which there was a significant inverse correlation between ejection fraction, the amount of myocardial fibrosis and apoptosis.

To determine if the amount of expression of any specific cytokine correlated with cardiac function as measured by ejection fraction, we first analyzed all 111 cytokines included in **Supplemental Table 1**. Of these, 34 cytokines showed significant up- or down-regulation when comparing WT vs. *Dsg2*$^{mut/mut}$ mice and/or untreated vs. Bay 11-7082-treated *Dsg2*$^{mut/mut}$ mice. We then assessed cytokine expression levels in each individual animal to determine if expression of any of these 34 cytokines correlated with cardiac function as measured by ejection fraction. Of these 34 molecules, the levels of LIX (CXCL5) and osteopontin (OPN) both showed a significant inverse correlation with ejection fraction (**Figure 6**) and a significant positive correlation with myocardial injury (percent fibrosis and apoptosis) and with each other (**Supplemental Figure 3**).

We then created a Pearson's correlation matrix to characterize the relationship between levels of LIX and OPN and the 32 other cytokines reported above. Levels of both LIX and OPN showed

significant correlations with 7 other cytokines: CCL21, complement factor D, DPP-IV, GAS6, IFNγ, IL-1Ra and IL-27 (**Supplemental Figure 3**). As discussed below, this network of cytokines regulates fundamental features of the inflammatory response including apoptosis, fibrosis and remodeling of the extracellular matrix. Taken together, these observations clearly implicate NFκB-mediated cytokine production as drivers of the ACM disease phenotype.

ACM patient iPSC-cardiac myocytes express abundant cytokines under the control of NFκB

It is not possible to identify and quantify the relative contributions of the innate immune response in cardiac myocytes vs. activation of inflammatory signaling in professional immune cells in studies in *Dsg2*$^{mut/mut}$ mice presented in Figures 3-6. It is likely that both play a role in the pathogenesis of the disease phenotype. However, to gain further insights into the immune response in cardiac myocytes in ACM, and to determine if this occurs as a cell autonomous mechanism in patients with ACM, we characterized immunoreactive signal for phospho-RelA/p65 (Ser536) and cytokine production in cultures of cardiac myocytes derived from hiPSCs obtained from a patient with documented ACM caused by a mutation in the desmosomal gene *PKP2*. These cultures are composed of more than 95% pure cardiac myocytes, and they are devoid of lymphocytes and macrophages. As shown in **Figure 7**, when grown under basal conditions in the absence of any provocative stimuli used in previous studies to induce various features of the ACM phenotype,[33] these cells displayed marked nuclear accumulation of phospho-RelA/p65 (Ser536) indicating activation of NFκB signaling pathways. They also expressed and secreted into the culture medium large amounts of cytokines including essentially all that were expressed in the hearts of *Dsg2*$^{mut/mut}$ mice. Exposure of ACM patient hiPSC-cardiac myocytes to Bay 11-7082 prevented nuclear accumulation of phospho-RelA/p65 and greatly reduced the amount of cytokines in cells and culture media (**Figure 7**). No nuclear signal for phospho-RelA/p65 (Ser536) was seen in control hiPSC-CMs including those treated with Bay 11-7082 under identical conditions nor was there any change in the distribution of plakoglobin (**Supplemental Figure 4**). **Supplemental Tables 2**

and 3 show data for all cytokines measured in control and patient hiPSC-cardiac myocytes and in their culture media. These observations provide additional independent evidence of activation of an innate immune response in cardiac myocytes in ACM under the control of NFκB signaling.

Discussion

ACM is a complex disease characterized by early onset of arrhythmias followed by progressive myocardial damage that can lead to heart failure.[1-3] Exactly how mutations in desmosomal genes cause such a complex clinical picture is incompletely understood but increasing evidence implicates abnormal activation of Wnt/β-catenin signaling via GSK3β.[4-6] The fact that SB216763, a small molecule inhibitor of GSK3β, can reverse both the myocardial injury and arrhythmia components of ACM shows that a common pathway drives the clinically important features of the disease.[6,8] Now, we provide new evidence that this pathway also involves inflammatory signaling. First, we showed that NFκB signaling is activated in three different experimental models of ACM involving expression of three different desmosomal gene variants known to cause disease in patients. This conclusion is based on observing increased expression and nuclear accumulation of phospho-RelA/p65, which are hallmarks of activation of the NFκB signaling cascade.[16,17] Such changes in phospho-RelA/p65 were blocked by Bay 11-7082, thus confirming that it acts to inhibit NFκB signaling. Next, we showed that Bay 11-7082 has a remarkable ability to rescue the full ACM phenotype both in vitro and in a robust mouse model in vivo. Taken together, these observations provide new insights into immune mechanisms in the pathogenesis of ACM and identify potential new therapeutic strategies to limit myocardial damage and reduce the risk of serious arrhythmias in patients with ACM.

The immune response in ACM consists of two components, both of which likely contribute to disease pathogenesis. The first component, infiltration of the myocardium by "professional" cells of the adaptive immune response (lymphocytes and macrophages), is the most conspicuous. Indeed, inflammatory cells can be so abundant in the hearts of ACM patients that the disease may be

misdiagnosed as myocarditis.[34] However, it has never been clear if inflammatory cells accumulate in the heart in ACM only as a reparative response to myocardial damage or if such cells actually promote arrhythmias and/or myocyte injury mediated by immune mechanisms. The second component involves activation of an innate immune response in cardiac myocytes in ACM. How this occurs is unclear although it is known that activation of GSK3β promotes inflammation through NFκB signaling.[18-21] In any event, we show here that NFκB signaling is activated in cardiac myocytes that express variants in three different desmosomal genes known to cause ACM in patients. These cardiac myocytes produce and secrete large amounts of diverse chemical mediators of the immune response in a cell autonomous fashion. Many are powerful chemoattractant molecules that likely mobilize bone marrow-derived inflammatory cells to the heart. Cardiac myocytes in ACM also produce powerful pro-inflammatory mediators such as IL-1β and TNFα, both of which are considered primordial cytokines of the innate immune response. This suggests that activation of immune signaling within cardiac myocytes may play an important role in driving the key clinical features of the disease. It also raises the interesting possibility that cytokines secreted by cardiac myocytes act in an autocrine fashion to alter ion channel function and promote arrhythmias in ACM. If so, this would add to the traditional view of the role of inflammation in arrhythmogenesis which holds that cardiac ion channel dysfunction is mediated by cytokines produced by lymphocytes and macrophages that infiltrate the heart in myocarditis or other inflammatory heart diseases.[35]

One striking observation in this study is the production and secretion of diverse pro-inflammatory cytokines and chemoattractants by ACM patient-derived cardiac myocytes grown under basal conditions in vitro. In previous studies of such cell lines,[33] it was necessary to use a combination of provocative stimuli (dexamethasone, 3-isobutyl-1-methylxanthine, rosiglitazone and indomethacin) to induce metabolic changes seen in patients with ACM. By contrast, we show that expression of a common pathogenic variant in *PKP2* is sufficient to activate NFκB signaling and induce marked

expression of immune mediators by human cardiac myocytes under basal conditions and in the absence of inflammatory cells. These observations provide further evidence that ACM disease alleles activate an innate immune response in cardiac myocytes independent of the actions of professional inflammatory cells.

Although our results to do not prove that cytokines are responsible for causing myocardial damage and arrhythmias in ACM, there was a clear correlation between activation of an immune response and expression of the disease phenotype. Expression levels of two cytokines in particular, LIX (CXCL5) and osteopontin (OPN), were found to correlate with ejection fraction in *Dsg2*$^{mut/mut}$ mice. LIX was increased by >50-fold in *Dsg2*$^{mut/mut}$ mice and its level was markedly reduced in ACM mice treated with Bay 11-7082. Production of LIX is stimulated by IL-1β and TNFα. It promotes chemotaxis of neutrophils and also plays a role in fibrosis. OPN expression was increased by >40-fold in *Dsg2*$^{mut/mut}$ mice and it too was reduced by Bay 11-7082. OPN regulates cell adhesion and survival. It also acts as a Th1 cytokine and participates in cell-mediated immune responses. In turn, expression of LIX and OPN was correlated with expression of other mediators including CCL21 (a T-cell and dendritic cell attractant), complement factor D (required for activation of the alternative pathway), DPP-IV (a dipeptidyl peptidase involved in immune regulation and apoptosis), GAS6 (which plays a role in fibrosis), IFNγ, IL-1Ra and IL-27 (which induces T-cell differentiation and upregulates IL-10 which itself was increased in ACM mice). These observations suggest that networks of immune mediators, likely derived from both cardiac myocytes and infiltrating inflammatory cells, interact in a complex fashion to promote the ACM disease phenotype.

Our results raise the possibility that targeting immune signaling could be an effective mechanism-based therapy in ACM. This notion is in keeping with recent insights into the role of immune activation in coronary artery disease and heart failure. For example, long-term use of canakinumab, a monoclonal antibody against IL-1β significantly reduced major adverse cardiac events

in patients with coronary artery disease in the CANTOS trail.[36] The fact that IL-1β expression was increased by ~13-fold in in *Dsg2*$^{mut/mut}$ mice warrants further investigation as a possible therapeutic strategy in ACM. Finally, strenuous exercise is known to accelerate disease penetrance and increase arrhythmic risk in ACM patients.[37,38] It remains to be determined if exercise intensifies the immune response in ACM and, if so, whether anti-inflammatory therapy might mitigate its adverse effects.

Acknowledgments

This work was supported by grants from St. Jude Medical (2015-2016 Heart Rhythm Society Cardiac Pacing and Electrophysiology Fellowship Award) and The Aiding Hearts Foundation (to SPC); an American Heart Association Transformational Project Award (18TPA34170559, to SPC and JES); grants from the Gilead Research Scholars in Cardiovascular Disease Fund and the British Heart Foundation (PG/18/27/33616) (to AA); an American Heart Association Pre-doctoral Fellowship Award (to JL); NICHD/NIH (1R01HD086026) and TEDCO (2015-MSCRFI-1622) grants (supporting PA); and NIH grant 5R01 HL120959 (to LT). We gratefully acknowledge support for the statistical analysis from the National Center for Research Resources and the National Center for Advancing Translational Sciences (NCATS) of the National Institutes of Health through grant number 1UL1TR001079.

References

1. Sen-Chowdhry S, Morgan RD, Chambers JC, McKenna WJ. Arrhythmogenic cardiomyopathy: etiology, diagnosis, and treatment. *Annu Rev Med.* 2010; 61:233-53.

2. Basso C, Bauce B, Corrado D, Thiene G. Pathophysiology of arrhythmogenic cardiomyopathy. *Nat Rev Cardiol.* 2012; 9:223-33.

3. Corrado D, Link M, Calkins H. Arrhythmogenic right ventricular cardiomyopathy. *New Eng J Med.* 2017; 376:61-72.

4. Garcia-Gras E, Lombardi R, Giocondo MR, Willerson JT, Schneider MD, Khoury DS, Marian AJ. Suppression of canonical Wnt/beta-catenin signaling by nuclear plakoglobin recapitulates phenotype of arrhythmogenic right ventricular cardiomyopathy. *J Clin Invest.* 2006; 116:2012-21.

5. Lombardi R, da Graca Cabreira-Hansen M, Bell A, Fromm RR, Willerson JT, Marian AJ. Nuclear plakoglobin is essential for differentiation of cardiac progenitor cells to adipocytes in arrhythmogenic right ventricular cardiomyopathy. *Circ Res*. 2011;109:1342-53.

6. Chelko SP, Asimaki A, Andersen P, Bedja D, Amat-Alarcon N, DeMazumder D, Jasti R, MacRae CA, Leber R, Kleber AG, Saffitz JE, Judge DP. Central role for GSK3β in the pathogenesis of arrhythmogenic cardiomyopathy. *JCI Insight*. 2016; 1(5). pii: e85923.

7. Coghlan MP, Culbert AA, Cross DA, Corcoran SL, Yates JW, Pearce NJ, Rausch OL, Murphy GJ, Carter PS, Roxbee Cox K. Mills D, Brown MJ, Haigh D, Ward RW, Smith DG, Murray KJ, Reith AD, Holder JC. Selective small molecule inhibitors of glycogen synthase kinase-3 modulate glycogen metabolism and gene transcription. *Chem Biol*. 2000; 7:793-803.

8. Asimaki A, Kapoor S, Plovie E, Karin Arndt A, Adams E, Liu Z, James CA, Judge DP, Calkins H, Churko J, Wu JC, MacRae CA, Kléber AG, Saffitz JE. Identification of a new modulator of the intercalated disc in a zebrafish model of arrhythmogenic cardiomyopathy. *Sci Transl Med*. 2014; 6:240ra74.

9. Asimaki A, Protonotarios A, James CA, Chelko SP, Tichnell C, Murray B, Tsatsopoulou A, Anastasakis A, te Riele A, Kleber AG, Judge DP, Calkins H, Saffitz JE: Characterizing the molecular pathology of arrhythmogenic cardiomyopathy in patient buccal mucosa cells. *Circ Arrhythm Electrophysiol.* 2016; 9: e003688.

10. Zhan T, Rindtorff N, Boutros M: Wnt signaling in cancer. *Oncogene.* 2017; 36:1461-1473.

11. Marcus FI, Fontaine GH, Guiraudon G, Frank R, Laurenceau JL, Malergue C, Grogogeat Y. Right ventricular dysplasia: a report of 24 adult cases. *Circulation.* 1982;65:384-398.

12. Fontaine G, Fontaliran F, Andrade FR, Velasquez E, Tonet J, Jouven X, Fujioka Y, Frank R. The arrhythmogenic right ventricle. Dysplasia versus cardiomyopathy. *Heart Vessels.* 1995; 10:227-235.

13. Corrado D, Basso C, Thiene G, McKenna WJ, Davies MJ, Fontaliran F, Nava A, Silvestri F, Blomstrom-Lundqvist C, Wlodarska EK, Fontaine G, Camerini F. Spectrum of clinicopathologic manifestations of arrhythmogenic right ventricular cardiomyopathy/dysplasia: a multicenter study. *J Am Coll Cardiol*. 1997; 30:1512–1520.

14. Lopez-Ayala JM, Pastor-Quirante F, Gonzalez-Carrillo J, Lopez-Cuenca D, Sanchez-Munoz JJ, Oliva-Sandoval JR, Gimeno JR. Genetics of myocarditis in arrhythmogenic right ventricular dysplasia. *Heart Rhythm*. 2015; 12:766-773.

15. Asimaki A, Tandri H, Duffy ER, Winterfield JR, Mackey-Bojack S, Picken MM, Cooper LT, Wilber DJ, Marcus FI, Basso C, Thiene G, Tsatsopoulou A, Protonotarios N, Stevenson WG, McKenna WJ, Gautam S, Remick DG, Calkins, Saffitz JE. Altered desmosomal proteins in granulomatous myocarditis and potential pathogenic links to arrhythmogenic right ventricular cardiomyopathy. *Circ Arrhyth Electrophysiol*. 2011; 4:743-52.

16. Campbell JJ, Perkins ND. Regulation of NF-kappaB function. *Biochem Soc Symp*. 2006; 73:165 180.

17. Hayden MS, Ghosh S. Shared principles in NF-kappaB signaling. *Cell*. 2008; 132:344-362.

18. Takada Y, Fang X, Jamaluddin MS, Boyd DD, Aggarwal BB. Genetic deletion of glycogen synthase kinase-3beta abrogates activation of IkappaBalpha kinase, JNK, Akt, and p44/p42 MAPK but potentiates apoptosis induced by tumor necrosis factor. *J Biol Chem*. 2004; 279:39541-39554.

19. Fiol CJ, Williams JS, Chou CH, Wang QM, Roach PJ, Andrisani OM. A secondary phosphorylation of CREB341 at Ser129 is required for the cAMP-mediated control of gene expression. A role for glycogen synthase kinase-3 in the control of gene expression. *J Biol Chem*. 1994; 269:32187 32193.

20. Bullock BP, Habener JF. Phosphorylation of the cAMP response element binding protein CREB by cAMP dependent protein kinase A and glycogen synthase kinase-3 alters DNA binding affinity, conformation, and increases net charge. *Biochemistry*. 1998; 37:3795-3809.

21. Martin M, Rehani K, Jope RS, Michalek SM. Toll-like receptor-mediated cytokine production is differentially regulated by glycogen synthase kinase 3. *Nat Immunol*. 2005; 6:777-784.

22. Dai Y, Pei XY, Rahmani M, Conrad DH, Dent P, Grant S. Interruption of the NF-kappaB pathway by Bay 11-7082 promotes UCN-01-mediated mitochondrial dysfunction and apoptosis in human multiple myeloma cells. *Blood*. 2004; 103:2761-2770.

23. Strickson S, Campbell DG, Emmerich CH, Knebel A, Plater L, Ritorto MS, Shpiro N, Cohen P. The anti-inflammatory drug BAY 11-7082 suppresses the MyD88-dependent signalling network by targeting the ubiquitin system. *Biochem J*. 2013; 451:427-437

24. Zhao J, Zhang H, Huang Y, Wang H, Wang S, Zhao C, Liang Y, Yang N. Bay11-7082 attenuates murine lupus nephritis via inhibiting NLRP3 inflammasome and NF-κB activation. *Int Immunopharmacol*. 2013; 17:116-122.

25. Wang F, Liu S, Du T, Chen H, Li Z, Yan J. NF-κB inhibition alleviates carbon tetrachloride-induced liver fibrosis via suppression of activated hepatic stellate cells. *Exp Ther Med.* 2014; 8:95-99.

26. Cong W, Ruan D, Xuan Y, Niu C, Tao Y, Wang Y, Zhan K, Cai L, Jin L, Tan Y. Cardiac-specific overexpression of catalase prevents diabetes-induced pathological changes by inhibiting NF-κB signaling activation in the heart. *J Mol Cell Cardiol.* 2015; 89:314-325.

27. Val-Blasco A, Prieto P, Gonzalez-Ramos S, Benito G, Vallejo-Cremades MT, Pacheco I, Gonzalez-Peramato P, Agra N, Terron V, Delgado C, Martin-Sanz P, Bosca L, Fernandez-Velasco M. NOD1 activation in cardiac fibroblasts induces myocardial necrosis in a murine model of type 2 diabetes. *Biochem J.* 2017; 474:399-410.

28. Syed F, Diwan A, Hahn HS. Murine echocardiography: a practical approach for phenotyping genetically manipulated and surgically modeled mice. *J Am Soc Echocardiogr.* 2005; 18:982-990.

29. Ong CS, Fukunishi T, Zhang H, Huang CY, Nashed A, Blazeski A, DiSilvestre D, Vricella K, Conte J, Tung L, Tomaselli GF, Hibino N. Biomaterial-free three-dimensional bioprinting of cardiac tissue using human induced pluripotent stem cell derived cardiomyocytes. *Sci Rep.* 2017; 7:4566.

30. Bhattacharya S, Burridge PW, Kropp EM, Chuppa SL, Kwok WM, Wu JC, Boheler KR, Gundry RL. High efficiency differentiation of human pluripotent stem cells to cardiomyocytes and characterization by flow cytometry. *J Vis Exp*. 2014; 91:52014.

31. McKoy G, Protonotarios N, Crosby A, Tsatsoupoulou A, Anastasakis A, Coonar A, Norman M, Baboonian C, Jeffery S, McKenna WJ. Identification of a deletion in plakoglobin in arrhythmogenic right ventricular cardiomyopathy with palmoplantar keratoderma and woolly hair (Naxos disease). *Lancet.* 2000; 355:2119-2124.

32. Asimaki A, Tandri J, Huang H, Halushka MK, Gautam S, Basso C, Thiene G, Tsatsopoulou A, Protonotarios N, McKenna WJ, Calkins H, Saffitz JE. A new diagnostic test for arrhythmogenic right ventricular cardiomyopathy. *New Eng J Med*. 2009; 360:1075-84.

33. Kim C, Wong J, Wen J, Wang S, Wang C, Spiering S, Kan NG, Forcales S, Puri PL, Leone TC, Marine JE, Calkins H, Kelly DP, Judge DP, Chen HS. Studying arrhythmogenic right ventricular dysplasia with patient-specific iPSCs. *Nature.* 2013; 494:105-110.

34. Basso C, Thiene G, Corrado D, Angelini A, Nava A, Valente M. Arrhythmogenic right ventricular cardiomyopathy. Dysplasia, dystrophy or myocarditis? *Circulation.* 1996; 94:983-991.

35. Lazzerini PE, Capecchi PL, Laghi-Pasini F. Systemic inflammation and arrhythmic risk: lessons from rheumatoid arthritis. *Eur Heart J.* 2017; 38:1717-1727.

36. Ridker PR, Everett BM, Thuren T, MacFayden JG, Chang WH, Ballantyne C, Forseca F, Nicolau J, Koenig W, Anker SD, Kastelein JJP, Cornel JH, Pais P, Pella D, Genest J, Cifkova R, Lorenzatti A, Forster T, Kobalava Z, Vida-Simiti L, Flather M, Shimokawa H, Ogawa H, Dellborg M, Rossi PRF,

Troquay RPT, Libby P, Glynn RJ, CANTOS trial group. Anti-inflammatory therapy with canakinumab for atherosclerotic disease. *N Eng J Med*. 2017;377:1119-1131.

37. James, CA, Bhonsale A, Tichnell C, Murray D. Russell SD, Tandri H, Tedford RJ, Judge DP, Calkins H. Exercise increases age-related penetrance and arrhythmic risk in arrhythmogenic right ventricular dysplasia/cardiomyopathy-associated desmosomal mutation carriers. *J Am Coll Cardiol*. 2013;62:1290-1297.

38. Rojas A, Calkins H. Present understanding of the relationship between exercise and arrhythmogenic right ventricular dysplasia/cardiomyopathy. *Trends Cardiovasc Med*. 2015; 25:181-188.

Figure Legends

Figure 1. Activation of NFκB and reversal of ACM features by Bay 11-7082 in neonatal rat ventricular myocytes (NRVMs) expressing a deletion mutation in the gene for plakoglobin (*JUP* ^{2157del2}). **A.** Representative confocal immunofluorescence images from control (non-transfected) NRVMs and NRVMs expressing *JUP* ^{2157del2} in the absence or presence of Bay 11-7082 showing the distribution of phospho-RelA/p65 (pRelA/p65). Nuclear accumulation of immunoreactive signal, indicating activation of NFκB, is readily apparent in cells expressing *JUP* ^{2157del2} (asterisks) but is absent in such cells after treatment with Bay 11-7082. Scale bar = 50μm. **B.** Representative confocal immunofluorescence images from control (non-transfected) NRVMs, and NRVMs expressing *JUP* ^{2157del2} in the absence or presence of Bay 11-7082. Arrows show localization of immunoreactive signal at the cell surface. The normal distribution of N-cadherin in all cells is shown as a positive control. Untreated *JUP* ^{2157del2} cells showed abnormal distribution of plakoglobin, Cx43 and GSK3β. The amount of signal for plakoglobin and Cx43 at cell-cell junctions was greatly reduced in these cells whereas signal for GSK3β, which normally resides in the cytoplasm, was seen at the cell surface. Asterisks identify apparent nuclear localization of plakoglobin in *JUP* ^{2157del2} cells. The abnormal distribution of plakoglobin, Cx43 and GSK3β was normalized in *JUP* ^{2157del2} cells treated with Bay 11-7082. Scale bar = 50μm. **C.** TUNEL labeling in control NRVMs, and NRVMs expressing *JUP* ^{2157del2} in the absence or presence of Bay 11-7082. Representative confocal images show increased TUNEL + nuclei (arrow heads) in cultures of cells expressing *JUP* ^{2157del2} and normalization after treatment with Bay 11-7082. Scale bar = 50μm. **D.** Graph showing the percent (%) apoptotic nuclei in 5 microscopic fields from each condition. * $P<0.0001$ for *JUP*^{2157del2} cells vs. control cells; † $P<0.0001$ for Bay 11-7082-treated vs. untreated *JUP*^{2157del2} cells determined by one-way ANOVA with Tukey's multiple comparisons test.

Figure 2. Bay 11-7082 reduces cytokines in the culture media in neonatal rat ventricular myocytes (NRVMs) expressing a deletion mutation in the gene for plakoglobin (*JUP* ^{2157del2}). Representative

cytokine arrays are shown for control (non-transfected) cells and NRVMs expressing *JUP* ^{2157del2} in the absence or presence of Bay 11-7082. The spots in the upper right and left and lower left corners are reference markers (Ref Bands) to compare overall exposure levels.

Figure 3. Activation of NFκB and reversal of ACM disease features in *Dsg2*$^{mut/mut}$ mice in vivo by inhibition of NFκB signaling with Bay 11-7082. A. Western blots of total RelA/p65 and phospho-RelA/p65 in homogenates of hearts from vehicle-treated wildtype (WT) mice, and vehicle- and Bay 11-7082-treated *Dsg2*$^{mut/mut}$ mice. **B.** Group data for total-RelA/p65 and pRelA/p65 (Ser536) protein levels in hearts of vehicle-treated WT mice, and vehicle- and Bay 11-7082-treated *Dsg2*$^{mut/mut}$ mice. **C.** Representative short-axis m-mode echocardiograms of vehicle-treated wildtype (WT) mice, *Dsg2*$^{mut/mut}$ mice and *Dsg2*$^{mut/mut}$ mice treated with Bay 11-7082. **D.** Group data for % ejection fraction in vehicle- and Bay 11-7082-treated wildtype (WT) mice, and vehicle- and Bay 11-7082-treated *Dsg2*$^{mut/mut}$ mice. **E.** Representative long-axis sections of the hearts stained with Masson trichrome from wildtype (WT) mice, *Dsg2*$^{mut/mut}$ mice and *Dsg2*$^{mut/mut}$ mice treated with Bay 11-7082. Scale bar = 1mm. **F.** Group data for % of left ventricular area occupied by fibrosis in Masson trichrome-stained sections of hearts from vehicle- and Bay 11-7082-treated wildtype (WT) mice, and vehicle- and Bay 11-7082-treated *Dsg2*$^{mut/mut}$ mice. **G.** Representative images showing TUNEL labeling in sections of hearts from wildtype (WT) mice, *Dsg2*$^{mut/mut}$ mice and *Dsg2*$^{mut/mut}$ mice treated with Bay 11-7082. Arrows show TUNEL+ nuclei. Scale bar = 10μm. **H.** Group data showing % apoptotic nuclei in TUNEL-labeled sections of hearts from vehicle- and Bay 11-7082-treated wildtype (WT) mice, and vehicle- and Bay 11-7082-treated *Dsg2*$^{mut/mut}$ mice. **I.** Representative signal-averaged electrocardiograms (SAECGs) from wildtype (WT) mice, *Dsg2*$^{mut/mut}$ mice and *Dsg2*$^{mut/mut}$ mice treated with Bay 11-7082. **J.** Representative confocal images of immunostained hearts from wildtype (WT) mice, *Dsg2*$^{mut/mut}$ mice and *Dsg2*$^{mut/mut}$ mice treated with Bay 11-7082. Arrows show localization of immunoreactive signal at the cell surface. The normal distribution of N-cadherin in all cohorts is shown as a positive control. Untreated

Dsg2$^{mut/mut}$ mice showed abnormal distribution of plakoglobin, Cx43, GSK3β and SAP97. The amount of signal for plakoglobin, Cx43 and SAP97 at cell-cell junctions was greatly reduced, whereas signal for GSK3β, which normally resides in the cytoplasm, was seen at the cell surface. These abnormal protein distributions were normalized in *Dsg2*$^{mut/mut}$ mice treated with Bay 11-7082. Scale bar = 10μm. Quantitative data in panels B, D, F and H are shown as mean ± SEM; n=10 for vehicle-treated WT mice; n=5 for Bay 11-7082-treated WT mice; n=9 for vehicle-treated *Dsg2*$^{mut/mut}$ mice; and n=17 for Bay 11-7082-treated *Dsg2*$^{mut/mut}$ mice. * P<0.001 for vehicle-treated *Dsg2*$^{mut/mut}$ mice vs. vehicle-treated WT mice; † P<0.001 for Bay 11-7082-treated *Dsg2*$^{mut/mut}$ mice vs. vehicle-treated *Dsg2*$^{mut/mut}$ mice as determined by one-way ANOVA with Tukey's multiple comparisons test.

Figure 4. Cytokine expression in the hearts of *Dsg2*$^{mut/mut}$ mice and its attenuation by Bay 11-7082. **A.** Representative cytokine arrays from hearts of vehicle-treated wildtype (WT) mice, *Dsg2*$^{mut/mut}$ mice and *Dsg2*$^{mut/mut}$ mice treated with Bay 11-7082. The spots in the upper right and left and lower left corners are reference markers (RBs) to compare overall exposure levels. **B.** Quantitative data for expression of selected cytokines in hearts of vehicle-treated wildtype (WT) mice, *Dsg2*$^{mut/mut}$ mice and *Dsg2*$^{mut/mut}$ mice treated with Bay 11-7082. Data are shown as mean ± SEM; n=5 for each cytokine in vehicle-treated WT and *Dsg2*$^{mut/mut}$ mice; n=10 for each cytokine in Bay11-7082-treated *Dsg2*$^{mut/mut}$ mice. * P<0.05 for any cohort vs. vehicle-treated WT mice; † P<0.05 for Bay 11-7082-treated *Dsg2*$^{mut/mut}$ mice vs. vehicle-treated *Dsg2*$^{mut/mut}$ mice as determined by one-way ANOVA with Tukey's multiple comparisons test.

Figure 5. Cytokine expression in cardiac myocytes and infiltrating inflammatory cells in hearts of *Dsg2*$^{mut/mut}$ mice. A. Representative immunoperoxidase stained sections of myocardium from vehicle-treated wildtype (WT) mice, *Dsg2*$^{mut/mut}$ mice and *Dsg2*$^{mut/mut}$ mice treated with Bay 11-7082 showing immunoreactive signal distributions for IL-1β, TNFα and MCP1α. Signal intensities for all 3 cytokines were increased in myocardial sections from *Dsg2*$^{mut/mut}$ mice. Signals for IL-1β and TNFα were seen in

both cardiac myocytes and infiltrating inflammatory cells in hearts of *Dsg2*$^{mut/mut}$ mice. Treatment with Bay 11-7082 reduced signal intensity. **B.** Immunoperoxidase stained sections of myocardium from *Dsg2*$^{mut/mut}$ mice showing the presence of both macrophages (CD68 + cells) and T-cells (CD3 + cells) (asterisks). Scale bar = 25 µm.

Figure 6. Correlations between cardiac function, myocardial injury and cytokine expression in *Dsg2*$^{mut/mut}$ mice. A. Pearson's correlation between cardiac function (ejection fraction) and myocardial fibrosis in *Dsg2*$^{mut/mut}$ mice treated with Bay 11-7082 (showing responders and non-responders). **B.** Pearson's correlation between cardiac function (ejection fraction) and myocardial apoptosis in *Dsg2*$^{mut/mut}$ mice treated with Bay 11-7082 (showing responders and non-responders). **C.** Pearson's correlation between cardiac function (ejection fraction) and myocardial fibrosis in vehicle-treated WT and *Dsg2*$^{mut/mut}$ mice, and *Dsg2*$^{mut/mut}$ mice treated with Bay 11-7082. **D.** Pearson's correlation between cardiac function (ejection fraction) and myocardial apoptosis in vehicle-treated WT and *Dsg2*$^{mut/mut}$ mice, and *Dsg2*$^{mut/mut}$ mice treated with Bay 11-7082). **E, F.** Pearson's correlation between expression levels of LIX (Panel E) and OPN (Panel F) and ejection fraction in each animal in all cohorts (vehicle-treated WT and *Dsg2*$^{mut/mut}$ mice, and *Dsg2*$^{mut/mut}$ mice treated with Bay 11-7082). Data in panels A-D are shown as mean ± SEM; n=10 for vehicle-treated WT mice; n=9 for vehicle-treated *Dsg2*$^{mut/mut}$ mice; and n=17 for *Dsg2*$^{mut/mut}$ mice treated with Bay 11-7082. Data in panels E, F are shown as mean ± SEM; n=5 for vehicle-treated WT and *Dsg2*$^{mut/mut}$ mice; n=8 for *Dsg2*$^{mut/mut}$ mice treated with Bay 11-7082. All correlation coefficients (r) and p-values were calculated using two-tailed Pearson's correlation analysis.

Figure 7. Activation of NFκB and cytokine expression in control and ACM patient derived hiPSC-cardiac myocytes. A. Representative confocal immunofluorescence images from cultures of cardiac myocytes (CMs) derived from a control hiPSC cell line and a line from an ACM patient with a pathogenic variant in plakophilin-2 (*PKP2*) grown in the absence or presence of Bay 11-7082. Virtually all *PKP2* cells are positive for cardiac troponin-I (cTnI) indicating they are cardiac myocytes. Control

hiPSC-CMs showed normal prominent cell surface staining for plakoglobin. Marked nuclear accumulation of immunoreactive signal for phospho-RelA/p65 (pRelA/p65) is seen in *PKP2* hiPSC CMs but not in control cells. Treatment of *PKP2* hiPSC CMs with Bay 11-7082 prevented nuclear accumulation of phospho-RelA/p65 signal. Scale bar = 20µm. **B.** Representative cytokine arrays prepared from cultures of cardiac myocytes derived from a control hiPSC cell line and a line from a patient with a disease causing variant in plakophillin-2 (*PKP2*). Arrays are shown for cells grown in the absence (untreated) or presence of Bay 11-7082. The spots in the upper right and left and lower left corners are reference markers (RBs) to compare overall exposure levels. **C.** Quantitative data (mean ± SEM; n=3 for each cohort and condition) for expression of selected cytokines in control and *PKP2* cells with or without Bay 11-7082. * $P<0.05$ for any cohort vs. control cardiac myocytes; † $P<0.05$ for Bay 11-7082-treated *PKP2* cardiac myocytes vs. untreated *PKP2* cardiac myocytes. **D.** Representative cytokine arrays prepared from culture media (supernatant) from cardiac myocytes derived from a control hiPSC cell line and a line from a patient with a disease causing variant in *PKP2.* Arrays are shown for media isolated from cells grown in the absence or presence of Bay 11-7082. The spots in the upper right and left and lower left corners are reference markers (RBs) to compare overall exposure levels. **E.** Quantitative data (mean ± SEM; n=3 for each cohort andcondition) for expression of selected cytokines in media from control and *PKP2* cells with or without Bay 11-7082. * $P<0.05$ for any cohort vs. control cardiac myocytes; † $P<0.05$ for Bay 11-7082 treated *PKP2* cardiac myocytes vs. untreated *PKP2* cardiac myocytes. Statistical analyses in panels C and E were performed using one-way ANOVA with Tukey's multiple comparisons test.

Table 1. Quantitative morphometric, echocardiographic and electrocardiographic data

Parameter	WT	WT + Bay11-7082	*Dsg2*$^{mut/mut}$	*Dsg2*$^{mut/mut}$ + Bay11-7082
Morphometric				
n	10	5	9	17
RWT (mm)	0.63 ± 0.02	0.67 ± 0.08	0.55 ± 0.04	0.64 ± 0.02
LVM (mg)	81.9 ± 4.9	87.9 ± 12.1	96.3 ± 6.03	92.9 ± 3.08
HW/BW (mg/g)	4.6 ± 0.2	4.8 ± 0.2	5.0 ± 0.2	4.7 ± 0.1
Echocardiography				
n	10	5	9	17
FS (%)	54.0 ± 1.5	53.1 ± 4.3	32.9 ± 3.4*†‡	49.5 ± 1.9
IVSd (mm)	0.88 ± 0.03‡	1.07 ± 0.2	0.91 ± 0.04‡	0.95 ± 0.02‡
LVIDd (mm)	2.87 ± 0.07	2.73 ± 0.26	3.22 ± 0.17	2.96 ± 0.06
LVIDs (mm)	1.32 ± 0.05	1.28 ± 0.18	2.16 ± 0.16*†‡	1.50 ± 0.08
Electrocardiography				
n	10	5	9	17
Heart Rate (bpm)	498 ± 12	464 ± 17†	506 ± 12	512 ± 12
RR-I (ms)	121 ± 2.8	130 ± 4.4†	119 ± 2.7	118 ± 2.5
PR-I (ms)	40.0 ± 0.9	44.1 ± 2.3	40.3 ± 1.6	39.0 ± 0.9
Pd (ms)	11.7 ± 0.2	10.1 ± 0.6	10.3 ± 0.6	10.1 ± 0.5
QRSd (ms)	12.5 ± 0.4	12.7 ± 0.7	13.8 ± 1.5†	11.4 ± 0.4
P-Amp (mV)	0.08 ± 0.01	0.07 ± 0.01	0.06 ± 0.01	0.06 ± 0.003*
R-Amp (mV)	0.84 ± 0.07	0.70 ± 0.03	0.55 ± 0.04*	0.66 ± 0.04*
Q-Amp (mV)	-0.03 ± 0.01	-0.03 ± 0.004	-0.11 ± 0.02*†‡	-0.06 ± 0.01
S-Amp (mV)	-0.25 ± 0.04	-0.16 ± 0.02	-0.042 ± 0.05*	-0.09 ± 0.04*

WT, wildtype; RWT, relative wall thickness; LVM, left ventricular mass; HW, heart weight; BW, body weight; FS, fractional shortening; IVSd, interventricular septum thickness at end-diastole; LVIDd, left ventricular internal diameter at end-diastole; LVIDs, left ventricular internal diameter at end-systole; RR-I, R-R interval; PR-I, P-R interval; Pd, P-wave duration; QRSd, QRS-wave duration; P-Amp, P-wave amplitude; R-Amp, R-wave amplitude; Q-Amp, Q-wave amplitude; S-Amp, S-wave amplitude. Data are shown as mean ± SEM; * P<0.05 for any cohort vs. vehicle-treated WT mice; † P<0.05 for any

cohort vs. Bay11-7082-treated *Dsg2*$^{mut/mut}$ mice; ‡ P<0.05 for any cohort vs. Bay11-7082-treated WT mice determined by one-way ANOVA with Tukey's multiple comparisons test.

Figure 1.

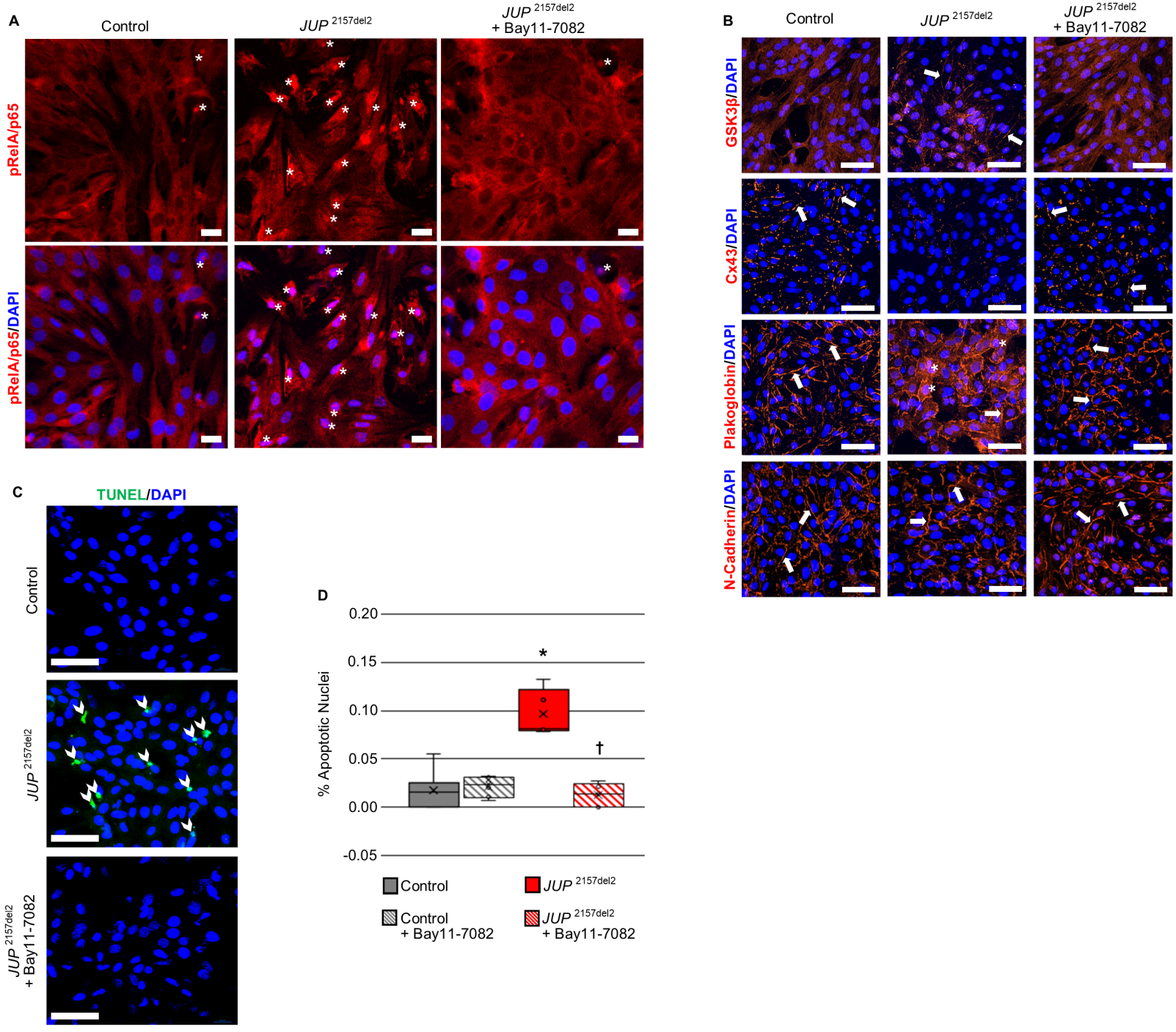
A
Control
JUP 2157del2
JUP 2157del2 + Bay11-7082
pRelA/p65
pRelA/p65/DAPI
B
Control
JUP 2157del2
JUP 2157del2 + Bay11-7082
GSK3β/DAPI
Cx43/DAPI
Plakoglobin/DAPI
N-Cadherin/DAPI
C
TUNEL/DAPI
Control
JUP 2157del2
JUP 2157del2 + Bay11-7082
D
% Apoptotic Nuclei
0.20
0.15
0.10
0.05
0.00
-0.05
*
†
Control
JUP 2157del2
Control + Bay11-7082
JUP 2157del2 + Bay11-7082

Figure 2.

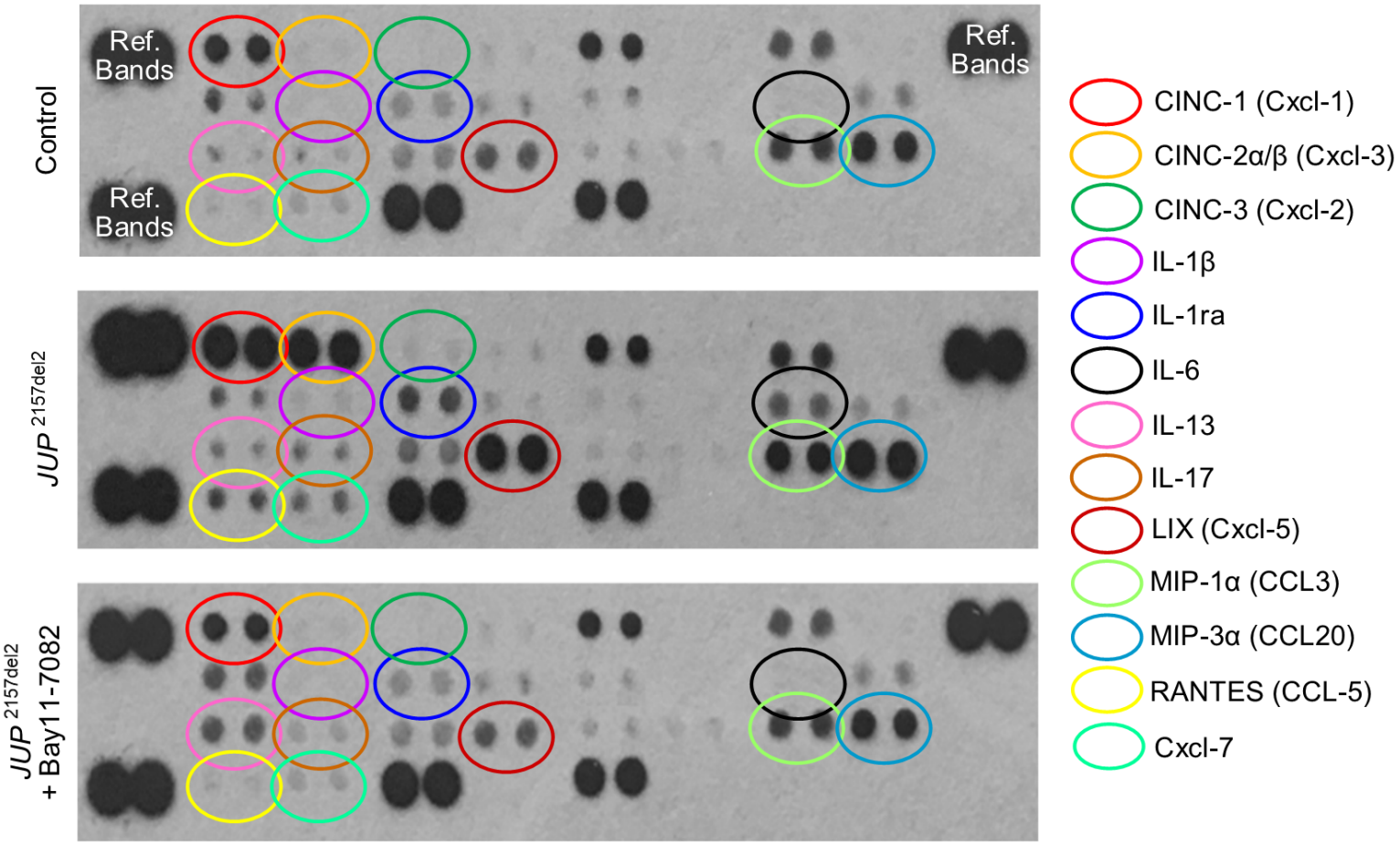
Control
Ref. Bands
Ref. Bands
Ref. Bands
Ref. Bands
JUP 2157del2
JUP 2157del2 + Bay11-7082
CINC-1 (Cxcl-1)
CINC-2α/β (Cxcl-3)
CINC-3 (Cxcl-2)
IL-1β
IL-1ra
IL-6
IL-13
IL-17
LIX (Cxcl-5)
MIP-1α (CCL3)
MIP-3α (CCL20)
RANTES (CCL-5)
Cxcl-7

Figure 3.

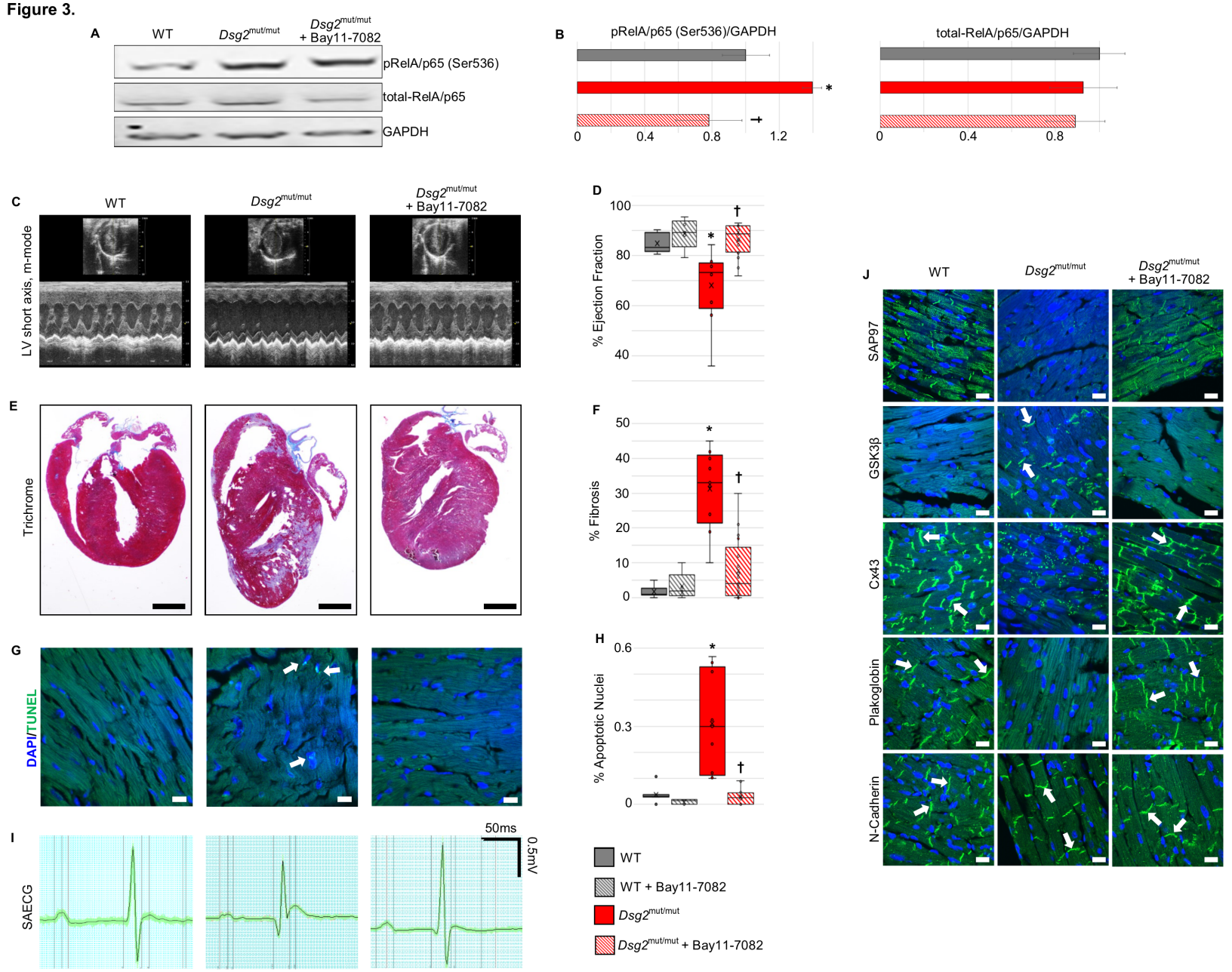
A
WT
Dsg2mut/mut
Dsg2mut/mut + Bay11-7082
pRelA/p65 (Ser536)
total-RelA/p65
GAPDH
B
pRelA/p65 (Ser536)/GAPDH
total-RelA/p65/GAPDH
0
0.4
0.8
1.2
C
LV short axis, m-mode
D
% Ejection Fraction
E
Trichrome
F
% Fibrosis
G
DAPI/TUNEL
H
% Apoptotic Nuclei
I
SAECG
50ms
0.5mV
WT
WT + Bay11-7082
Dsg2mut/mut
Dsg2mut/mut + Bay11-7082
J
SAP97
GSK3β
Cx43
Plakoglobin
N-Cadherin

Figure 4.

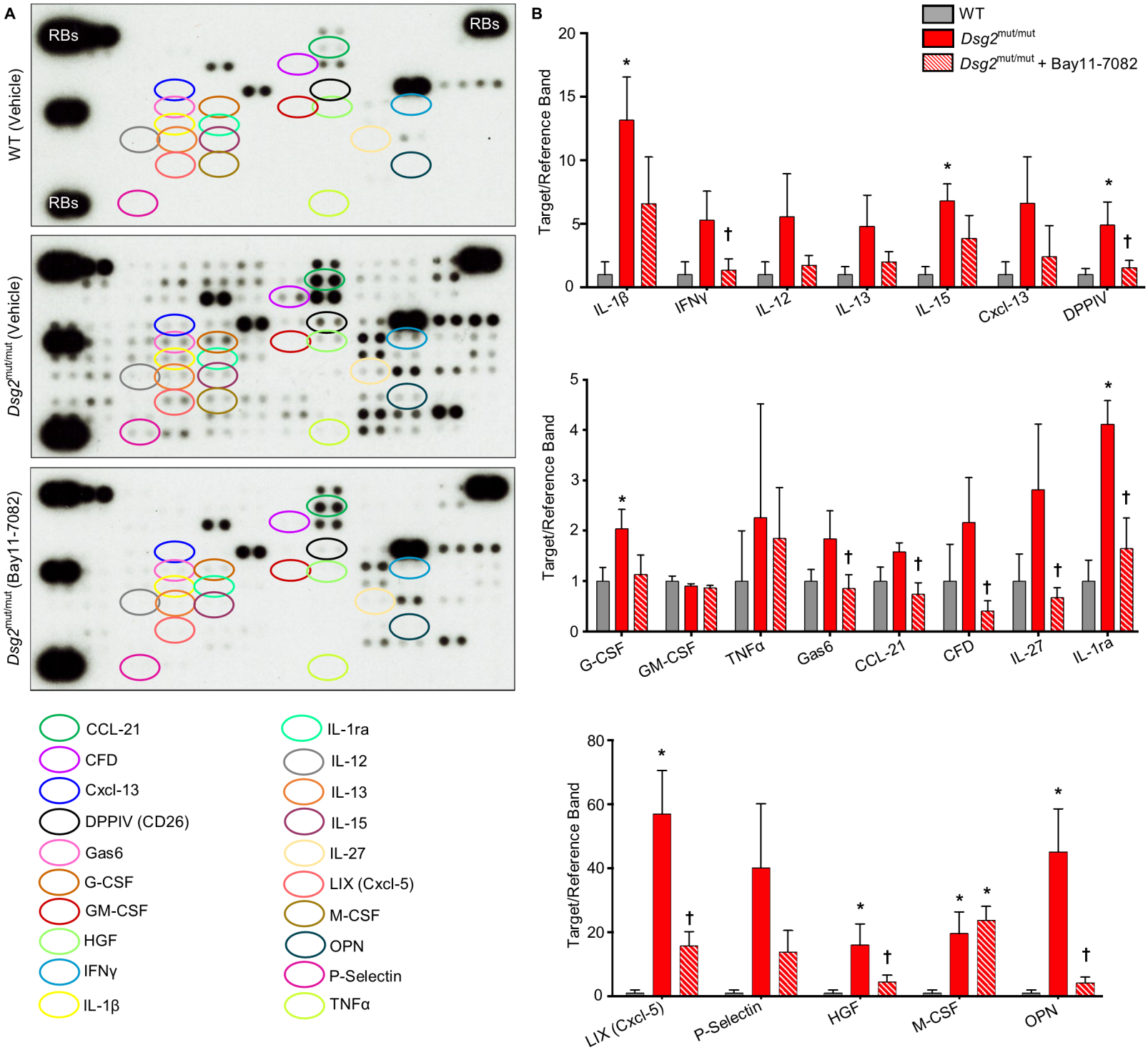
A
WT (Vehicle)
Dsg2mut/mut (Vehicle)
Dsg2mut/mut (Bay11-7082)
RBs
RBs
RBs
RBs
CCL-21
CFD
Cxcl-13
DPPIV (CD26)
Gas6
G-CSF
GM-CSF
HGF
IFNγ
IL-1β
IL-1ra
IL-12
IL-13
IL-15
IL-27
LIX (Cxcl-5)
M-CSF
OPN
P-Selectin
TNFα
B
WT
Dsg2mut/mut
Dsg2mut/mut + Bay11-7082
Target/Reference Band
IL-1β
IFNγ
IL-12
IL-13
IL-15
Cxcl-13
DPPIV
G-CSF
GM-CSF
TNFα
Gas6
CCL-21
CFD
IL-27
IL-1ra
LIX (Cxcl-5)
P-Selectin
HGF
M-CSF
OPN

Figure 5.

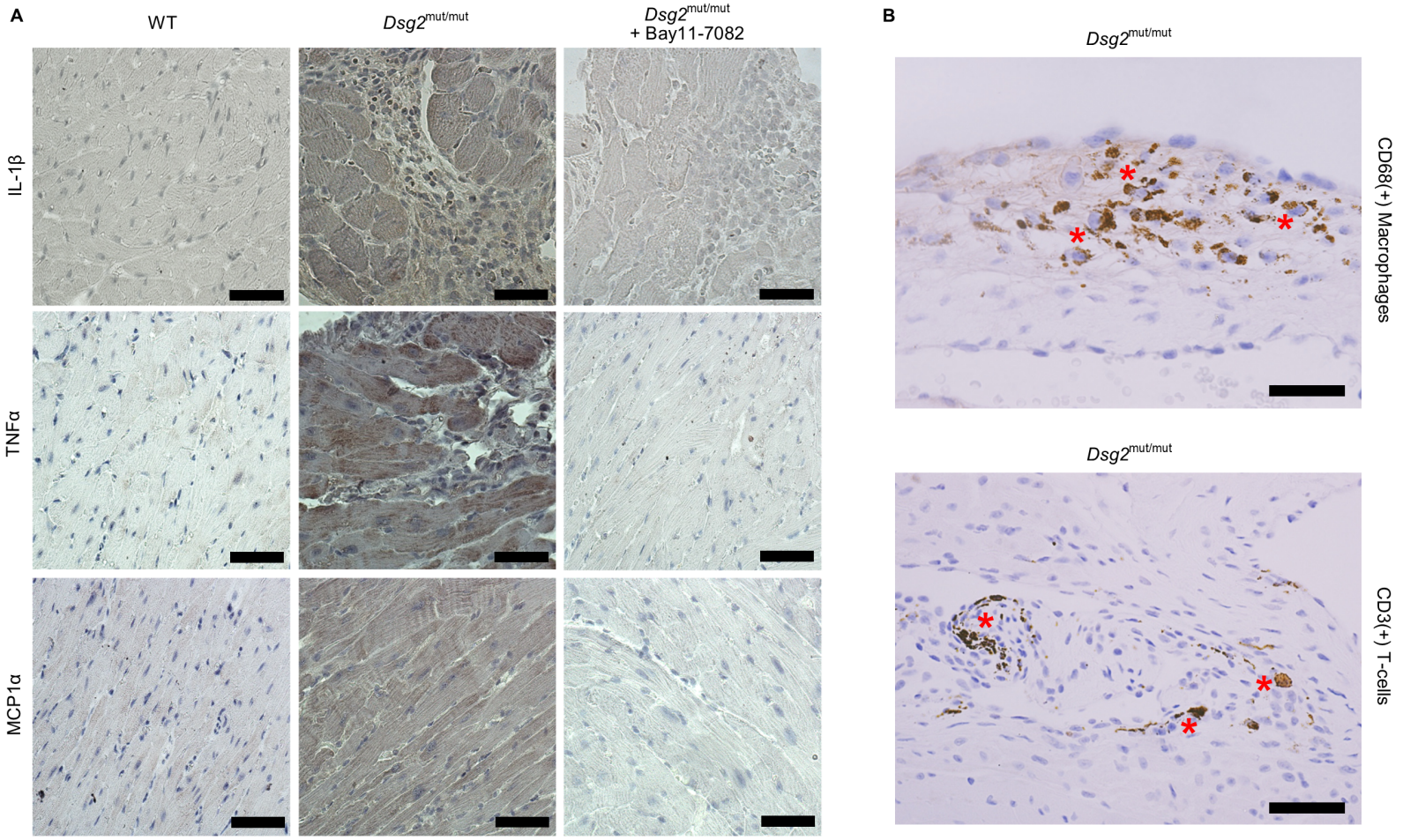
A
WT
Dsg2mut/mut
Dsg2mut/mut
+ Bay11-7082
IL-1β
TNFα
MCP1α
B
Dsg2mut/mut
CD68(+) Macrophages
Dsg2mut/mut
CD3(+) T-cells

Figure 6.

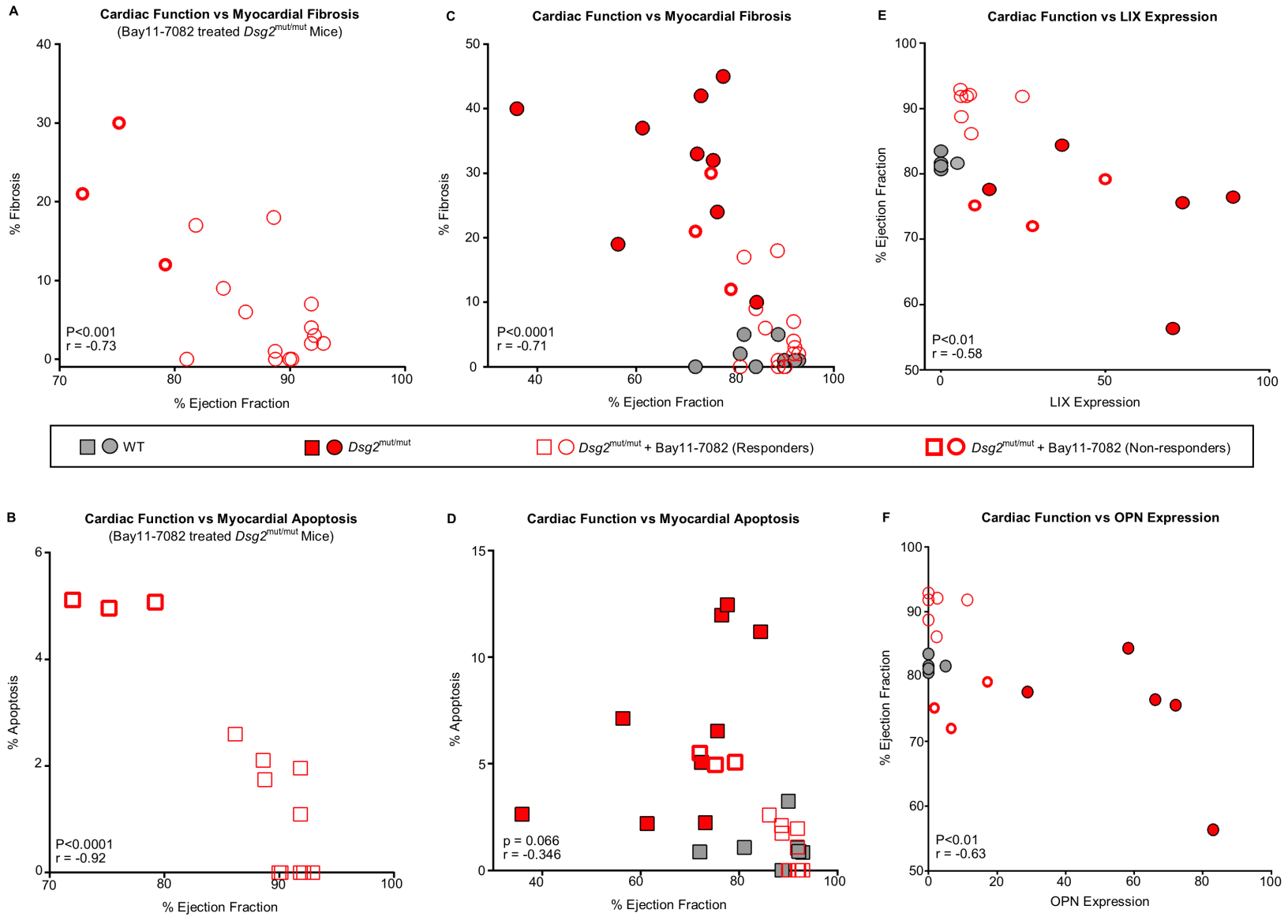
A
Cardiac Function vs Myocardial Fibrosis
(Bay11-7082 treated Dsg2mut/mut Mice)
% Fibrosis
% Ejection Fraction
P<0.001
r = -0.73
C
Cardiac Function vs Myocardial Fibrosis
% Fibrosis
% Ejection Fraction
P<0.0001
r = -0.71
E
Cardiac Function vs LIX Expression
% Ejection Fraction
LIX Expression
P<0.01
r = -0.58
WT
Dsg2mut/mut
Dsg2mut/mut + Bay11-7082 (Responders)
Dsg2mut/mut + Bay11-7082 (Non-responders)
B
Cardiac Function vs Myocardial Apoptosis
(Bay11-7082 treated Dsg2mut/mut Mice)
% Apoptosis
% Ejection Fraction
P<0.0001
r = -0.92
D
Cardiac Function vs Myocardial Apoptosis
% Apoptosis
% Ejection Fraction
p = 0.066
r = -0.346
F
Cardiac Function vs OPN Expression
% Ejection Fraction
OPN Expression
P<0.01
r = -0.63

Figure 7.

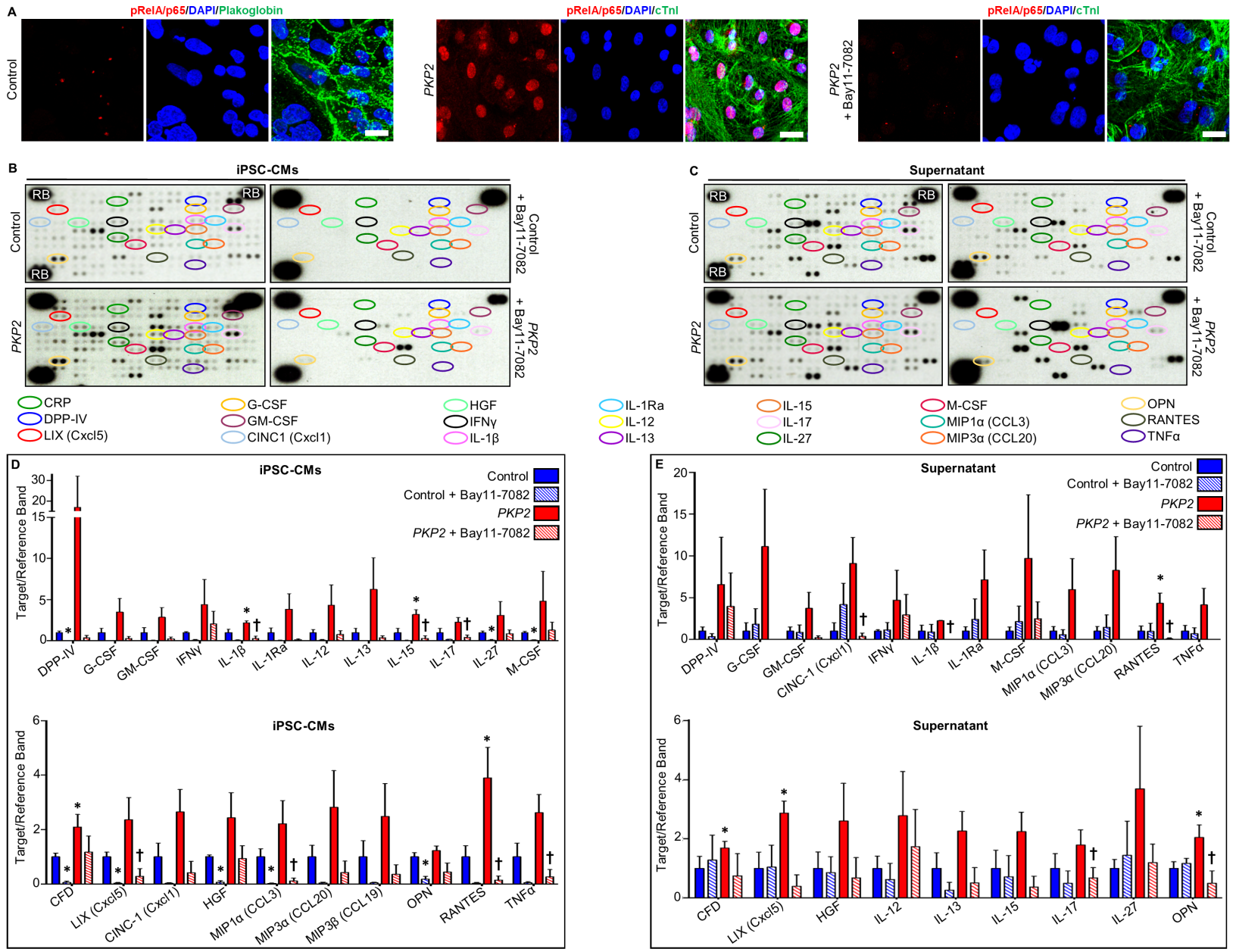
A
pRelA/p65/DAPI/Plakoglobin
pRelA/p65/DAPI/cTnI
pRelA/p65/DAPI/cTnI
Control
PKP2
PKP2 + Bay11-7082
B
iPSC-CMs
C
Supernatant
RB
Control
+ Bay11-7082
PKP2
CRP
DPP-IV
LIX (Cxcl5)
G-CSF
GM-CSF
CINC1 (Cxcl1)
HGF
IFNγ
IL-1β
IL-1Ra
IL-12
IL-13
IL-15
IL-17
IL-27
M-CSF
MIP1α (CCL3)
MIP3α (CCL20)
OPN
RANTES
TNFα
D
iPSC-CMs
E
Supernatant
Control
Control + Bay11-7082
PKP2
PKP2 + Bay11-7082
Target/Reference Band
CFD
MIP3β (CCL19)